ACS Photonics

Article

Cite This: ACS Photonics 2018, 5, 867−874

Engineering the Emission of Broadband 2D Perovskites by Polymer Distributed Bragg Reflectors

Paola Lova,[†,‡] Daniele Cortecchia,[†,‡] Harish N. S. Krishnamoorthy,[§] Paolo Giusto,[∥] Chiara Bastianini,[∥] Annalisa Bruno,[†] Davide Comoretto,*[,∥] and Cesare Soci*[,§]

[†]Energy Research Institute, Nanyang Technological University, 50 Nanyang Avenue, Singapore 639798

[‡]Interdisciplinary Graduate School, Nanyang Technological University, 21 Nanyang Link, Singapore 637371

[§]Centre for Disruptive Photonic Technologies, TPI, SPMS, Nanyang Technological University, 21 Nanyang Link, Singapore 637371

[∥]Dipartimento di Chimica e Chimica Industriale, Università di Genova, via Dodecaneso 31, 16146 Genova, Italy

Supporting Information

ABSTRACT: Thanks to their broadband emission and solution processability, 2D hybrid perovskite materials are promising for the realization of large area and flexible lighting devices. The deposition of 2D perovskites, however, requires wide range solvents that are incompatible with commodity polymers used for structural support and light management. Here we demonstrate coupling of broad-emitting 2,2-(ethylenedioxy)bis(ethylammonium)$PbCl_4$ perovskite with solution processed polymer distributed Bragg reflectors on both rigid fused silica and flexible polymer substrates. The optical functions of the chemically engineered perovskite were determined by ellipsometric measurements and used to design dielectric multilayer structures with photonic bandgap tunable over the entire visible range. The resulting photonic structures control directionality and spectral enhancement or suppression of the perovskite photoluminescence, in agreement with simple analytical optical models. These results pave the way to the development of a new generation of color-tunable light-emitting devices based on a single active material.

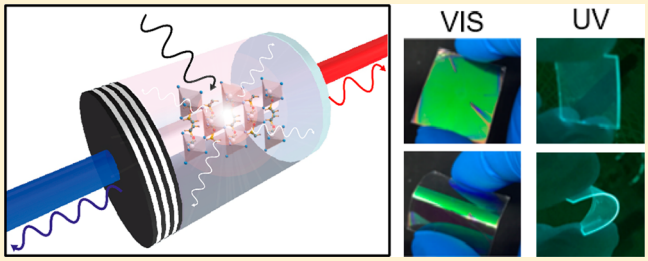

KEYWORDS: *2D hybrid perovskites, broadband luminescence, light management, polymer distributed Bragg reflectors (DBRs), hybrid multilayered structures*

Organo-lead halide perovskites are attracting considerable fundamental and technological interest due to their potential as efficient light-emitting[1,2] and photovoltaic materials.[3−9] Indeed, perovskite-based photovoltaic devices have already been commercialized.[10−12] The compatibility of perovskite film synthesis and deposition with solution-based fabrication techniques has opened up the possibility to manufacture a variety of low-cost optoelectronic devices besides photovoltaic cells, which include solid state lasers, light-emitting diodes, and transistors.[13−17] Moreover, a variety of perovskite materials, with wide range of optoelectronic properties underlying device operation, have been synthesized by simple compositional design.[12,13,18,19] Among these, 2D perovskite structures with general formula 2,2′-(ethylenedioxy)bis-(ethylammonium), where X = Cl or Br ((EDBE)PbX_4, Figure 1a) are considered particularly appealing due to their broadband photoluminescence (PL) spectrum.[20−24] In particular, it is thought that broad-emitting 2D perovskites could be employed as the active layer in flexible large area light-emitting devices, where compositional tuning may be replaced by light emission engineering in compatible photonic structures.[13,21,25−27]

The spontaneous emission properties of an emitter can be altered by engineering the photonic environment surrounding it.[28,29] Photonic structures such as distributed Bragg reflectors (DBRs) and microcavities are the most commonly used approaches to accomplish this task due to spectral and directional redistribution of the photoluminescence oscillator strength.[30] Polymer multilayered structures have been widely employed for efficient enhancement and suppression of fluorescence of organic dyes.[31−39] Only recently, solution-based processes for the encapsulation of inorganic nanocrystals in polymer photonic structures[38] made plastic devices suitable to control the luminescence properties of inorganic and hybrid emitters as well. Integration of solution-processed perovskite films into photonic crystal structures made of commodity polymers would be the natural next step. Fabrication of multilayered dielectric lattices from solution can be accomplished by techniques like spin-coating[32−34,40,41] and dip-coating[42,43] of polymers or inorganic nanoparticles and by block copolymer self-assembly.[44] While block copolymer self-assembly requires complicated and expensive synthesis

Received: September 17, 2017
Published: January 21, 2018

DOI: 10.1021/acsphotonics.7b01077
ACS Photonics 2018, 5, 867−874

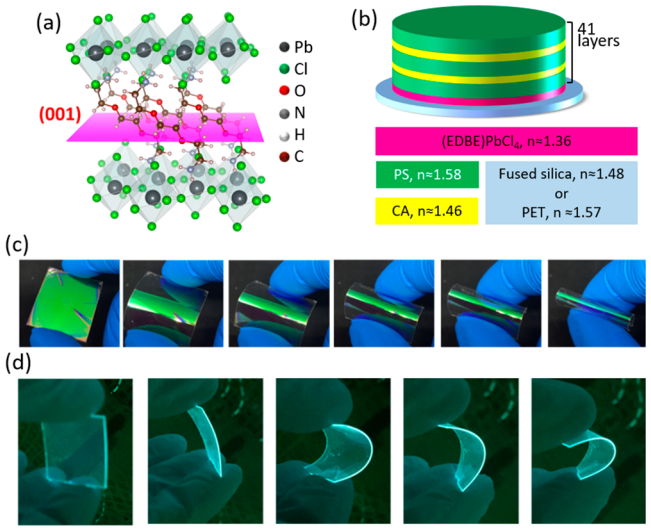

Figure 1. (a) Crystalline structure of the $(EDBE)PbCl_4$ perovskite, the magenta plane indicates the (001) crystalline plane in the $(EDBE)PbCl_4$ structure.[20] (b) Schematic of the $(EDBE)PbCl_4$ DBR. (c, d) Photograph of the $(EDBE)PbCl_4$ DBR cast on flexible PET substrate under visible (c) and ultraviolet (350 nm, panel d) illumination. The images from left to right illustrate the flexibility of the all-polymer DBR under mechanical bending.

routes,[45,46] the assembly of inorganic nanoparticles necessitates time-consuming postdeposition annealing.[47−51] On the other hand, polymer processing is a fast and low cost technique to produce free-standing and flexible devices, which can be readily scaled-up using existing industrial packaging technologies.[52,53]

Spun-cast polymer microcavities and DBRs have been extensively used to control lasing and directional enhanced spontaneous emission.[31−34,36−38,54,55] In most realizations, the emitter is either embedded within a defect of the periodic photonic crystal structure[32,33] or used as an active dielectric component of the photonic crystal lattice[31,56,57] to achieve cavity-mode or band-edge emission enhancement, respectively. Unfortunately, as most of solution-processable perovskite films, $(EDBE)PbCl_4$ can only be cast by wide range solvents, which would dissolve most polymers. This makes the deposition of $(EDBE)PbCl_4$ within DBRs or microcavities, made of polymer thin films, very challenging. To overcome this issue, we fabricated a photonic crystal structure where $(EDBE)PbCl_4$ is first cast on 50 μm thick polyethylene terephthalate (PET) sheets and on fused silica substrate. The polymer DBR multilayer was subsequently grown over the perovskite film to create a half planar microcavity (Figure 1b). Figure 1c,d shows a series of photographs of the flexible DBR cast on PET collected under visible light and ultraviolet illumination. We demonstrate that this structure allows directional and spectral redistribution of the $(EDBE)PbCl_4$ broadband photoluminescence. We first discuss the structural and optical properties of the $(EDBE)PbCl_4$ thin films, and then focus on the modification of their spontaneous emission properties when coupled to the flexible DBRs made of commodity polymers. The DBR structures are made of polystyrene and cellulose acetate[58] and designed for optimal spectral overlap between the photonic band gap (PBG) and the $(EDBE)PbCl_4$ broad emission. Spectral and intensity distributions of the photoluminescence collected from either side of the multilayer stack are reproduced by simple optical models based on the transfer matrix formalism.

RESULTS AND DISCUSSION

The two-dimensional $(EDBE)PbCl_4$ crystal structure consists of single layers of highly distorted $PbCl_6$ octahedra linked to each other by a layer of ordered 2,2′(ethylenedioxy)bis-(ethylammonium) ditopic cations (Figure 1a).[20,21,59] The perovskite is grown by spin-coating a stoichiometric solution of $(EDBE)Cl_2$ and $PbCl_2$ in dimethyl sulfoxide (DMSO), and further annealing at 100 °C (see Methods). This process facilitates growth of perovskite films with thicknesses ranging from 20 nm to a few microns and with roughness down to 3 nm (Figure 2a and Supporting Information, Figures S1 and S2).

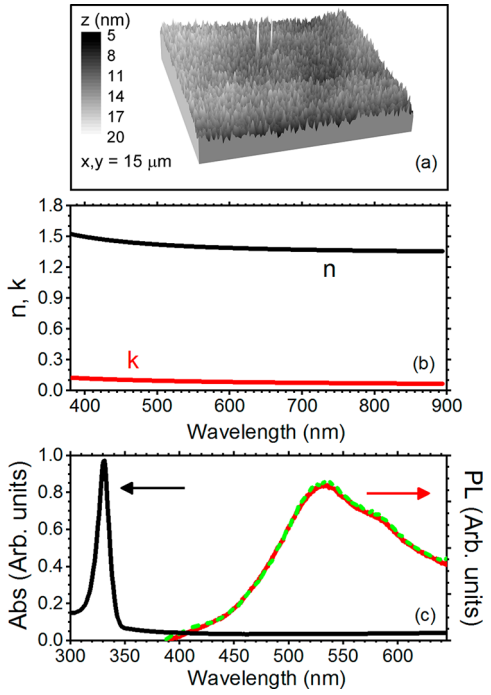

Figure 2. Morphological and optical properties of the $(EDBE)PbCl_4$ thin film spun-cast on fused silica from solution with concentration 0.1 M: (a) Three-dimensional topography of the film retrieved from atomic force microscopy data; (b) Spectral response of the real (n, black line) and imaginary (k, red line) parts of the refractive index; (c) Absorbance (black line) and emission spectra collected from the front (red continuous line) and back (green dashed line) sample surfaces.

The X-ray diffraction pattern reported in Supporting Information, Figure S3, shows that perovskite layers are strongly oriented toward the ⟨100⟩ direction, in agreement with previous reports.[21,23,24]

In this work, we used perovskite films with thickness of 40 nm. Figure 2b displays the real and the imaginary parts of the film optical constants determined by ellipsometry (see Methods), which were then used to design the DBRs. The refractive index far from the resonance approaches 1.35. This low value is probably due to the low density of the layered system. Only below 500 nm the refractive index increases, while absorption is negligible within the investigated spectral range. Figure 2c compares the absorbance and photoluminescence spectra of the perovskite thin film. The $(EDBE)PbCl_4$ absorption (black line) shows a sharp peak with a maximum at 335 nm, while its broad photoluminescence spectrum (Figure 2c, red line) extends from 400 to ∼750 nm and has a maximum of intensity at ∼530 nm, which decreases at larger tilting angles (Supporting Information, Figure S5). Such broad

DOI: 10.1021/acsphotonics.7b01077
ACS Photonics 2018, 5, 867−874

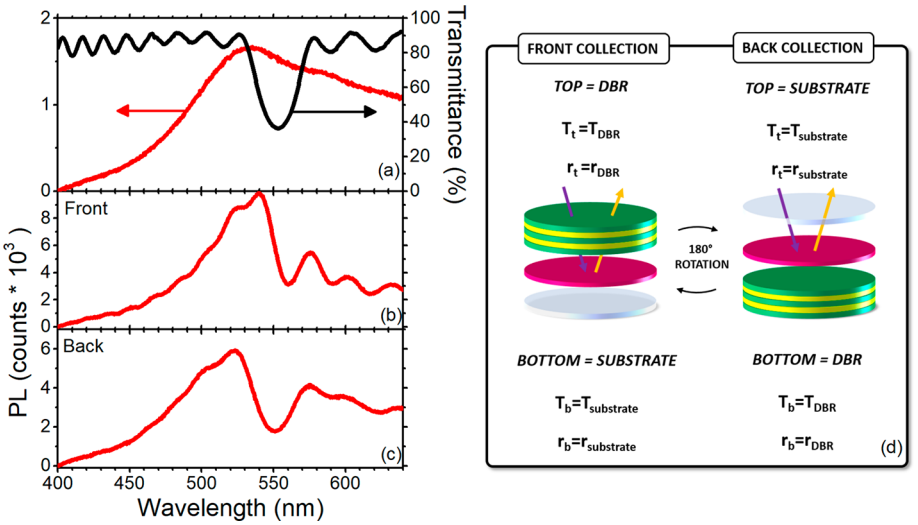

Figure 3. (a) Measured transmittance spectrum of an $(EDBE)PbCl_4$ DBR with stop-band centered at 560 nm (black line) and PL spectrum of bare $(EDBE)PbCl_4$ film (red line) spun cast on fused silica substrate. $(EDBE)PbCl_4$ emission intensity collected from the front (b) and back (c) sides of the multilayer stack (DBR stop-band cantered at 560 nm). (d) Schematics of the front and back collection configuration used in photoluminescence measurements.

emission is an intrinsic property of the 2D perovskite, which derives from the formation of self-trapped excitons, involving the localization of holes and electrons at specific sites of the inorganic lattice as small polarons.[21,23,24,60,61]

The optical constants of the perovskite film reported in Figure 2b, along with previously measured data for polystyrene and cellulose acetate,[62] were used to design three DBRs with stop-bands overlapping the perovskite emission spectrum. The $(EDBE)PbCl_4$ film thickness and roughness obtained with different deposition conditions were evaluated by atomic force microscopy (see Methods and Supporting Information, Figures S1 and S2). A schematic of the architecture is shown in Figure 1b. Figure 1c,d shows actual photographs of an $(EDBE)PbCl_4$ DBR cast on flexible PET substrate, a video showing the flexibility of the all-polymer DBR under mechanical bending is also available as Supporting Information. Because PET, like many commercial polymers, absorbs and emits light in the same spectral region as $(EDBE)PbCl_4$, detailed analysis of the optical response of the DBR was performed using UV transparent fused silica substrates. The optical characterization of the flexible samples is reported in Supporting Information, Figure S4. Supporting Information, Figure S5, shows the calculated and experimental transmittance spectra for the three DBRs cast on fused silica substrate with PBG centered at 505, 560, and 590 nm. All measured transmittance spectra show a minimum at wavelength corresponding to the stop-band, and a Fabry-Pérot pattern due to the interference of the transmitted/reflected beams from the top and bottom surfaces of the DBRs, in full agreement with calculations. Figure 3 compares the experimental transmittance data of the samples with PBG centered at 560 nm with the PL spectrum of the perovskite film (see also Figure 2) and with the emission of the film coupled with the DBR. We report the data collected from the front and bottom surfaces of the multilayer sample (see schematics of the two collection configurations in Figure 3d). The data for the other two samples, with DBR PBG centered at 505 and 590 nm, are available in Supporting Information, Figure S6. For the bare $(EDBE)PbCl_4$ thin film, the shape and intensity of the PL spectrum is identical when recorded in the front or back collection configurations (Figures 2c and 3a). Conversely, when the perovskite film is coupled to the DBR, the PL spectra collected from the front surface (with the substrate facing the collection side, Figure 3b) and from the back surface (with the DBR facing the collection side, Figure 3c) display major differences. We first notice that the PL intensity of the spectrum recorded from the substrate side (front geometry, Figure 3b) is more intense than for the DBR side (back geometry, Figure 3b). Moreover, irrespectively of the collection configuration, the emission spectra measured from the perovskite film coupled to the DBR are by far more intense than those recorded for the bare perovskite film (Figure 3a). While the emission intensity collected in the back configuration is suppressed within the PBG region (Figure 3b), the photoluminescence collected in the front configuration is enhanced at the low wavelength side of the DBR PBG (Figure 3c). This suggests that the DBR behaves as a mirror for front detection, and as a filter for back detection. An identical behavior is observed in the other two samples (Supporting Information, Figure S6). The effects leading to the emission enhancement and its spectral shift with respect to the stop-band will be discussed in the following (Figure 5 and related discussion).

The characteristic spectral features induced by the coupling of the $(EDBE)PbCl_4$ with the DBR are strongly dependent on the collection angle (Supporting Information, Figures S4 and S8), in agreement with the photonic band structure of DBRs (see refs63 and 64 and references therein reported). Since the anisotropy of the perovskite layer (see Supporting Information, Figure S3) and the DBR structure may affect angle dependent measurements for different polarizations,[65,66] all measurements were performed using unpolarized light, which allows capturing the main effect of the DBR on the perovskite fluorescence without complicated polarization sensitive excitation and detection schemes.[67−69] Figure 4 shows the angular dispersion of the ratio between the PL emitted by the perovskite coupled to the DBR with PBG centered at 560 nm and the PL of the perovskite reference sample ($PL_{DBR}/PL_{thin\ film}$). The different data sets were also normalized to account for the different extraction efficiency accordingly to the literature (see ref 70 and references reported therein). For detection in the back

DOI: 10.1021/acsphotonics.7b01077
ACS Photonics 2018, 5, 867−874

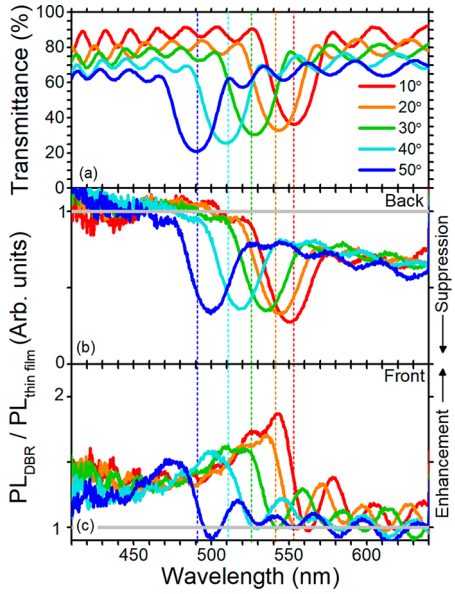

Figure 4. Angle resolved transmittance and normalized PL spectra of (EDBE)$PbCl_4$ coupled to the DBR with PBG centered at 560 nm. Transmittance (a) and normalized photoluminescence intensity measured in the back (b) and front (c) collection configurations. All spectra were collected at 10° (red), 20° (yellow), 30° (green), 40° (cyan), and 50° (blue). The colored dashed lines indicate the spectral position of the PBG for the five collection angles.

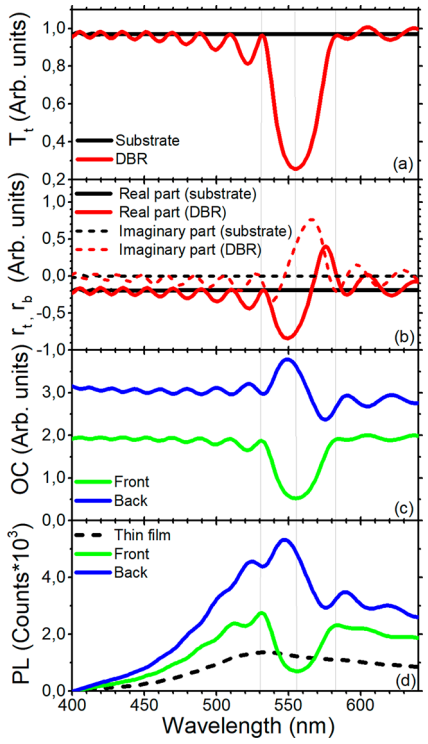

Figure 5. Transmittance spectra calculated for the bare DBR sample (red line) and for the fused silica substrate (black line). (b) Real (continuous lines) and imaginary (dashed lines) parts of the Fresnel reflection coefficients for the bare DBR (red lines) and for the fused silica substrate (black lines). (c) OC factors calculated for light collection form the two DBR sides: front collection in blue and back collection in green (refer to Figure 3d for collection geometry). Calculated (EDBE)$PbCl_4$ emission spectra for front (green line) and back (blue line) collection, and measured photoluminescence of (EDBE)$PbCl_4$ thin film on fused silica substrate (black dashed line). All spectra are calculated via the transfer matrix method as previously reported,[38] for a collection angle of $\theta = 10°$.

configuration (red line in Figure 4b), the fingerprint of the PBG is observed in the normalized PL spectrum as a dip positioned at ∼550 nm, with amplitude smaller than one. This feature is slightly red-shifted with respect to the PBG shown in the transmittance spectrum of Figure 4a, which is positioned at 555 nm. This minimum in relative PL intensity shows that light propagation is forbidden for photon wavelengths within the PBG region. On the long wavelength side of the PBG, the relative PL intensity remains lower than one (PL of the perovskite coupled to the DBR is suppressed), while one would expect a value of the order of unity. Based on the simulations discussed later on, this is due to different light out-coupling efficiency from the front and back sides of the DBR (eq 2 and Figure 5b). For increasing detection angle, the dip in the emission spectrum blue shifts, according to the angular dispersion properties of the DBR. When collected from the front side of the sample, the intensity of the PL spectrum is strongly asymmetric (red line in Figure 4c). The maximum of the relative PL emission intensity is blue-shifted by ∼20 nm with respect to the stop-band (red dashed line in Figure 4). Moving to longer wavelengths, the signal strongly decreases in correspondence of the DBR stop-band, then evolves into a Fabry−Perot interference pattern with average intensity close to unity. Similar behavior is observed in the two samples with different PBG, both in the front and back detection configuration (Supporting Information, Figure S7).

To develop a quantitative understanding of the spectral PL enhancement/suppression induced by the DBR in the front and back measuring configurations, we calculated the out-coupling (OC) factor and the PL spectra of the (EDBE)$PbCl_4$ film coupled with the DBR at the two perovskite interfaces. Neglecting orientation effects and emission lifetime, in a system where the emitter is placed within a nonabsorbing DBR and a partially reflecting surface (the substrate), the OC factor depends on the transmittance of the top medium (T_t) and on the amplitude of the electric field reflected by the media at the emitter interfaces ($r_b r_t$):[71]

$$\mathrm{OC} = n_e \xi \frac{2T_t}{|1 - r_b r_t e^{2ikd}|^2} \quad (1)$$

where n_e is the emitter refractive index, k is the wavenumber, L is the thickness of the emitting layer and position, and ξ is the antinode factor, which equals 1 for an emitter homogeneously distributed within the emitting layer.[39,71] To model the OC factor, we first calculated the transmittance (Figure 5a) and the Fresnel reflection coefficients (Figure 5b, real part) at the angle of incidence of $\theta = 10°$ for a self-standing fused silica substrate (red line) and a DBR with the normal-incidence stop-band centered at ∼560 nm (black lines). The Fresnel reflection coefficient of the DBR is highly asymmetric, which is attributed to two factors: (i) the optical thickness of the polystyrene and cellulose acetate layers does not fulfill the $\lambda/4$ condition, and (ii) the first polystyrene layer grown on the perovskite has a considerably different thickness (see Methods) than the layers spun-cast on cellulose acetate with the same velocity and solution concentration due to the different friction endured. These factors affect the spectral out-coupling from the two sides of the sample. Indeed, the OC factor shows a minimum at the long wavelength side of the PBG for front detection, while a broader maximum is observed in the back detection

DOI: 10.1021/acsphotonics.7b01077
ACS Photonics 2018, 5, 867−874

configuration. Therefore, the shape of the PL spectrum, which is given by the product between PL_{ref} and the calculated OC factor, is strongly dependent on the detection configuration (Figure 5d). As anticipated, the differences in PL spectral shape are dictated by T and r. When the emission is collected from the front side, since the transmittance of fused silica $T_t \approx 1$, the OC factor is mainly influenced by the Fresnel reflection coefficients of the DBR, whereas for back-side collection (where DBR is the top medium), it is affected by the DBR transmittance spectrum as well, which carries the spectral fingerprint of the PBG.

CONCLUSIONS

In summary, we demonstrated directional spectral redistribution of the spontaneous emission of broad-emitting 2D perovskite $(EDBE)PbCl_4$ embedded in flexible polymer DBRs. The coupled multilayered structures were fully processed from solution. Intensity and spectral shape of the PL recorded from the two sides of the structure are fully reproduced by a simple optical model based on transfer matrices, using the optical constants of $(EDBE)PbCl_4$ measured by ellipsometry as input parameters. Emission suppression and enhancement at specific wavelengths could be used to tune the emission color in light emitting devices comprising of a single broadband emitting active material. Thanks to the ease of fabrication and scalability of solution-processed multilayer structures, this approach could enable industrial scale production of low-cost, large area, lightweight, and flexible polymer-perovskite lighting devices, which may be tuned over the entire visible spectrum without resorting to compositional engineering.

METHODS

Sample Design and Fabrication. *$(EDBE)PbCl_4$ Synthesis.* $(EDBE)Cl_2$, where EDBE = 2,2′-(ethylenedioxy)bis-(ethylammonium), was synthesized by reaction of 2,2′-(ethylenedioxy)bis(ethylamine) (98%, Sigma-Aldrich) with 2 equiv of HCl (57% w/w in water, Sigma-Aldrich) for 2 h at 0 °C. The resulting white salt was purified by dissolving it in hot ethanol, followed by precipitation with diethyl ether (×3) and finally dried with a rotary evaporator and in vacuum oven overnight at 60 °C. The hybrid perovskite $(EDBE)PbCl_4$ was spun-cast at 4000 rpm for 60 s and annealed at 100 °C for 15 min. Thin films were fabricated from 0.1 M solutions prepared by mixing stoichiometric amounts of $(EDBE)Cl_2$ and $PbCl_2$ (99.999% trace metal basis, Aldrich) in dimethyl sulfoxide (anhydrous DMSO, Sigma-Aldrich). The perovskite deposition was performed in glovebox under N_2 environment.

DBR Design. Angle dependence of transmittance spectra for polymer DBRs were calculated using a Matlab home-written code based on the transfer matrix formalism.[39,40,62] Measured film thickness and refractive index dispersion were used as inputs.

DBR Preparation. Polymer multilayers were grown on top of a 40 nm $(EDBE)PbCl_4$ thin film deposed on fused silica or PET substrates by dynamic spin coting of alternate layers of polystyrene (M_w = 200000, n = 1.58) dissolved in toluene and cellulose acetate (M_w = 61000, n = 1.46) dissolved in diacetone alcohol. The polymer concentrations were ∼17 mg/mL for cellulose acetate and 35 mg/mL for polystyrene, and the rotation speed was kept between 4000 and 8000 rpm. The first polystyrene layer at the perovskite interface was deposed using identical conditions, but static spin-coating was employed. Polystyrene was used as the capping layer for the perovskite thin film due to the orthogonality between toluene and the $(EDBE)PbCl_4$. Indeed, toluene has been widely employed in solar cells as a solvent to cast hole transport layers on top of perovskite films.[72−74] The PS films also offers a barrier to the cellulose acetate solvent (diacetone alcohol), which does not dissolve polystyrene,[75] as demonstrated in our previous works.[38,40,58,62,76,77]

Optical and Morphological Characterization. *Optical Constants.* The optical constants of the perovskite were obtained by ellipsometric measurements of a 50 nm thick film on silicon substrate. Measurements were carried out in the range of 380−950 nm using the Woollam alpha Spectroscopic Ellipsometer. The real and imaginary parts of the optical constant of the perovskite film were determined by fitting the ellipsometry data to a Cauchy-Urbach model. In this model, the real part of the optical constant (n) is modeled using the Cauchy dispersion formula,

$$n = A + \frac{B}{\lambda^2} + \frac{C}{\lambda^4} \tag{2}$$

while the absorption in the UV region is described by an Urbach absorption tail, and the imaginary part (k) is modeled according to literature[78,79]

$$k = \alpha \cdot \beta e^{(E-\gamma)} \tag{3}$$

where the parameters A, B, C, α, and β are fit-parameters determined by modeling the ellipsometry data, λ is the wavelength in nm, E is the energy in eV, and γ (eV) is the band-edge parameter which is set equal to the largest energy in the measured data. The used parameters are A = 1.3361, B = 0.0141, C = 0.0019, α = 0.1262, β = 0.3326, and γ = 3.2522.

Morphological Characterization. The polymer and the perovskite film thicknesses and surface roughness were determined by atomic force microscopy (AFM) using a Scanning Probe Microscope Digital Instrument Dimension *V*.

Crystallographic Characterization. X-ray diffraction patterns of $(EDBE)PbCl_4$ were measured with a BRUKER D8 ADVANCE goniometer with Bragg−Brentano geometry using Cu Kα radiation (λ = 1.54056 Å). The measurements were collected with a step increment of 0.02° and 1 s acquisition time.

Optical Characterization. Angle resolved transmittance and photoluminescence spectra were contemporary collected coupling a Fluorolog Horiba endowed with a CCD detector and coupled with an Avantes AvaSpec-3046 spectrometer (200−1150 nm, resolution 1.4 nm). Photoluminescence spectra were collected in the range of 390−640 nm using the CCD, with excitation at 335 nm.

ASSOCIATED CONTENT

Supporting Information

The Supporting Information is available free of charge on the ACS Publications website at DOI: 10.1021/acsphotonics.7b01077.

$(EDBE)PbCl_4$ thin film characterization (Figures S1−S3), characterization of $(EDBE)PbCl_4$ DBRs cast on PET (Figure S4), and on fused silica (Figure S5). Effect of the DBRs on the $(EDBE)PbCl_4$ photoluminescence (Figures S6−S9) (PDF).

Video showing the flexibility of the all-polymer DBR under mechanical bending (AVI).

DOI: 10.1021/acsphotonics.7b01077
ACS Photonics 2018, 5, 867−874

AUTHOR INFORMATION

Corresponding Authors

*E-mail: davide.comoretto@unige.it.
*E-mail: csoci@e.ntu.edu.sg.

ORCID

Harish N. S. Krishnamoorthy: 0000-0001-6107-3383
Davide Comoretto: 0000-0002-2168-2851
Cesare Soci: 0000-0002-0149-9128

Notes

The authors declare no competing financial interest.

ACKNOWLEDGMENTS

Research conducted at NTU was supported by the Singapore Ministry of Education (Grant Nos. MOE2016-T1-1-164 and MOE2011-T3-1-005) and the Singapore National Research Foundation (CRP Award No. NRF-CRP14-2014-03). The work at UNIGE was funded by the Italian Ministry of University, Research and Instruction (Grant No. 2010XLLNM3). C.B. thanks the support of NTU's Summer Research Internship Programme and PG acknowledges the International Mobility Programme 2015/2016 of UNIGE supported by the Italian Ministry of the University, Research and Instruction. The authors thank Prof. Marina Alloisio and Prof. Andrea Basso (Dipartimento di Chimica e Chimica Industriale, Università di Genova) for their help and assistance with the characterization of flexible sample.

REFERENCES

(1) Stranks, S. D.; Snaith, H. J. Metal-halide perovskites for photovoltaic and light-emitting devices. *Nat. Nanotechnol.* **2015**, *10*, 391−402.
(2) D'Innocenzo, V.; Srimath Kandada, A. R.; De Bastiani, M.; Gandini, M.; Petrozza, A. Tuning the light emission properties by band gap engineering in hybrid lead halide perovskite. *J. Am. Chem. Soc.* **2014**, *136*, 17730−17733.
(3) Zhang, W.; Saliba, M.; Moore, D. T.; Pathak, S. K.; Hörantner, M. T.; Stergiopoulos, T.; Stranks, S. D.; Eperon, G. E.; Alexander-Webber, J. A.; Abate, A.; Sadhanala, A.; Yao, S.; Chen, Y.; Friend, R. H.; Estroff, L. A.; Wiesner, U.; Snaith, H. J. Ultrasmooth organic−inorganic perovskite thin-film formation and crystallization for efficient planar heterojunction solar cells. *Nat. Commun.* **2015**, *6*, 6142.
(4) NREL Research Cell Efficiency Records. http://www.nrel.gov/ncpv/ (accessed 10/09/2017).
(5) Gao, P.; Gratzel, M.; Nazeeruddin, M. K. Organohalide lead perovskites for photovoltaic applications. *Energy Environ. Sci.* **2014**, *7*, 2448−2463.
(6) Burschka, J.; Pellet, N.; Moon, S.-J.; Humphry-Baker, R.; Gao, P.; Nazeeruddin, M. K.; Gratzel, M. Sequential deposition as a route to high-performance perovskite-sensitized solar cells. *Nature* **2013**, *499*, 316−319.
(7) Zhou, H.; Chen, Q.; Li, G.; Luo, S.; Song, T.-b.; Duan, H.-S.; Hong, Z.; You, J.; Liu, Y.; Yang, Y. Interface engineering of highly efficient perovskite solar cells. *Science* **2014**, *345*, 542−546.
(8) Zhang, W.; Anaya, M.; Lozano, G.; Calvo, M. E.; Johnston, M. B.; Míguez, H.; Snaith, H. J. Highly efficient perovskite solar cells with tunable structural color. *Nano Lett.* **2015**, *15*, 1698−1702.
(9) Saliba, M.; Matsui, T.; Seo, J.-Y.; Domanski, K.; Correa-Baena, J.-P.; Nazeeruddin, M. K.; Zakeeruddin, S. M.; Tress, W.; Abate, A.; Hagfeldt, A.; Gratzel, M. Cesium-containing triple cation perovskite solar cells: improved stability, reproducibility and high efficiency. *Energy Environ. Sci.* **2016**, *9*, 1989−1997.
(10) Dyesol: http://www.dyesol.com/about-dyesol (accessed 20/07/2017).
(11) Oxford Photovoltaics: https://www.oxfordpv.com/Technology (accessed 20/07/2017).
(12) Solaronix: https://www.solaronix.com/news/ (accessed 20/07/2017).
(13) Xing, G.; Mathews, N.; Lim, S. S.; Yantara, N.; Liu, X.; Sabba, D.; Grätzel, M.; Mhaisalkar, S.; Sum, T. C. Low-temperature solution-processed wavelength-tunable perovskites for lasing. *Nat. Mater.* **2014**, *13*, 476−480.
(14) Gil-Escrig, L.; Longo, G.; Pertegas, A.; Roldan-Carmona, C.; Soriano, A.; Sessolo, M.; Bolink, H. J. Efficient photovoltaic and electroluminescent perovskite devices. *Chem. Commun.* **2015**, *51*, 569−571.
(15) Chin, X. Y.; Cortecchia, D.; Yin, J.; Bruno, A.; Soci, C. Lead iodide perovskite light-emitting field-effect transistor. *Nat. Commun.* **2015**, *6*, 7383.
(16) Deschler, F.; Price, M.; Pathak, S.; Klintberg, L. E.; Jarausch, D.-D.; Higler, R.; Hüttner, S.; Leijtens, T.; Stranks, S. D.; Snaith, H. J.; Atatüre, M.; Phillips, R. T.; Friend, R. H. High photoluminescence efficiency and optically pumped lasing in solution-processed mixed halide perovskite semiconductors. *J. Phys. Chem. Lett.* **2014**, *5*, 1421−1426.
(17) Cho, H.; Jeong, S.-H.; Park, M.-H.; Kim, Y.-H.; Wolf, C.; Lee, C.-L.; Heo, J. H.; Sadhanala, A.; Myoung, N.; Yoo, S.; Im, S. H.; Friend, R. H.; Lee, T.-W. Overcoming the electroluminescence efficiency limitations of perovskite light-emitting diodes. *Science* **2015**, *350*, 1222−1225.
(18) Boix, P. P.; Agarwala, S.; Koh, T. M.; Mathews, N.; Mhaisalkar, S. G. Perovskite solar cells: Beyond methylammonium lead iodide. *J. Phys. Chem. Lett.* **2015**, *6*, 898−907.
(19) Saparov, B.; Mitzi, D. B. Organic−inorganic perovskites: Structural versatility for functional materials design. *Chem. Rev.* **2016**, *116*, 4558−4596.
(20) Dohner, E. R.; Jaffe, A.; Bradshaw, L. R.; Karunadasa, H. I. Intrinsic white-light emission from layered hybrid perovskites. *J. Am. Chem. Soc.* **2014**, *136*, 13154−13157.
(21) Cortecchia, D.; Yin, J.; Bruno, A.; Lo, S.-Z. A.; Gurzadyan, G. G.; Mhaisalkar, S.; Bredas, J.-L.; Soci, C. Polaron self-localization in white-light emitting hybrid perovskites. *J. Mater. Chem. C* **2017**, *5*, 2771−2780.
(22) Dou, L.; Wong, A. B.; Yu, Y.; Lai, M.; Kornienko, N.; Eaton, S. W.; Fu, A.; Bischak, C. G.; Ma, J.; Ding, T.; Ginsberg, N. S.; Wang, L.-W.; Alivisatos, A. P.; Yang, P. Atomically thin two-dimensional organic-inorganic hybrid perovskites. *Science* **2015**, *349*, 1518−1521.
(23) Yin, J.; Li, H.; Cortecchia, D.; Soci, C.; Brédas, J.-L. Excitonic and polaronic properties of 2D hybrid organic−inorganic perovskites. *ACS Energy Lett.* **2017**, *2*, 417−423.
(24) Cortecchia, D.; Neutzner, S.; Srimath Kandada, A. R.; Mosconi, E.; Meggiolaro, D.; De Angelis, F.; Soci, C.; Petrozza, A. Broadband emission in two-dimensional hybrid perovskites: The role of structural deformation. *J. Am. Chem. Soc.* **2017**, *139*, 39−42.
(25) Gholipour, B.; Adamo, G.; Cortecchia, D.; Krishnamoorthy, H. N. S.; Birowosuto, M. D.; Zheludev, N. I.; Soci, C. Organometallic perovskite metasurfaces. *Adv. Mater.* **2017**, *29*, 1604268.
(26) Ramírez Quiroz, C. O.; Bronnbauer, C.; Levchuk, I.; Hou, Y.; Brabec, C. J.; Forberich, K. Coloring semitransparent perovskite solar cells via dielectric mirrors. *ACS Nano* **2016**, *10*, 5104−5112.
(27) Wang, J.; Cao, R.; Da, P.; Wang, Y.; Hu, T.; Wu, L.; Lu, J.; Shen, X.; Xu, F.; Zheng, G.; Chen, Z. Purcell effect in an organic-inorganic halide perovskite semiconductor microcavity system. *Appl. Phys. Lett.* **2016**, *108*, 022103.
(28) Yablonovitch, E. Inhibited spontaneous emission in solid-state physics and electronics. *Phys. Rev. Lett.* **1987**, *58*, 2059−2062.
(29) John, S. Strong localization of photons in certain disordered dielectric superlattices. *Phys. Rev. Lett.* **1987**, *58*, 2486−2489.
(30) Scotognella, F.; Varo, S.; Criante, L.; Gazzo, S.; Manfredi, G.; Knarr, R. J., III; Comoretto, D. *Organic and Hybrid Photonic Crystals*, 1st ed.; Springer International Publishing: Cham, CHZ, 2015; Vol. *1*, p 493.
(31) Scotognella, F.; Monguzzi, A.; Cucini, M.; Meinardi, F.; Comoretto, D.; Tubino, R. One dimensional polymeric organic photonic crystals for DFB lasers. *Int. J. Photoenergy* **2008**, *2008*, 1−4.

DOI: 10.1021/acsphotonics.7b01077
ACS Photonics 2018, 5, 867−874

(32) Canazza, G.; Scotognella, F.; Lanzani, G.; De Silvestri, S.; Zavelani-Rossi, M.; Comoretto, D. Lasing from all-polymer microcavities. *Laser Phys. Lett.* **2014**, *11*, 035804.
(33) Frezza, L.; Patrini, M.; Liscidini, M.; Comoretto, D. Directional enhancement of spontaneous emission in polymer flexible microcavities. *J. Phys. Chem. C* **2011**, *115*, 19939−19946.
(34) Gazzo, S.; Manfredi, G.; Pötzsch, R.; Wei, Q.; Alloisio, M.; Voit, B.; Comoretto, D. High refractive index hyperbranched polyvinylsulfides for planar one-dimensional all-polymer photonic crystals. *J. Polym. Sci., Part B: Polym. Phys.* **2016**, *54*, 73−80.
(35) Knarr, R. J., III; Manfredi, G.; Martinelli, E.; Pannocchia, M.; Repetto, D.; Mennucci, C.; Solano, I.; Canepa, M.; Buatier de Mongeot, F.; Galli, G.; Comoretto, D. In-plane anisotropic photoresponse in all-polymer planar microcavities. *Polymer* **2016**, *84*, 383−390.
(36) Fornasari, L.; Floris, F.; Patrini, M.; Comoretto, D.; Marabelli, F. Demonstration of fluorescence enhancement via bloch surface waves in all-polymer multilayer structures. *Phys. Chem. Chem. Phys.* **2016**, *18*, 14086−14093.
(37) Manfredi, G.; Mayrhofer, C.; Kothleitner, G.; Schennach, R.; Comoretto, D. Cellulose ternary photonic crystal created by solution processing. *Cellulose* **2016**, *23*, 2853−2862.
(38) Manfredi, G.; Lova, P.; Di Stasio, F.; Krahne, R.; Comoretto, D. Directional fluorescence spectral narrowing in all-polymer microcavities doped with CdSe/CdS dot-in-rod nanocrystals. *ACS Photonics* **2017**, *4*, 1761−1769.
(39) Lova, P.; Grande, V.; Manfredi, G.; Patrini, M.; Herbst, S.; Würthner, F.; Comoretto, D. All-Polymer photonic microcavities doped with perylene bisimide J-aggregates. *Adv. Opt. Mater.* **2017**, *5*, 1700523.
(40) Lova, P.; Bastianini, C.; Giusto, P.; Patrini, M.; Rizzo, P.; Guerra, G.; Iodice, M.; Soci, C.; Comoretto, D. Label-free vapor selectivity in poly(p-phenylene oxide) photonic crystal sensors. *ACS Appl. Mater. Interfaces* **2016**, *8*, 31941−31950.
(41) Mıguez, H.; Yang, S. M.; Ozin, G. A. Colloidal photonic crystal microchannel array with periodically modulated thickness. *Appl. Phys. Lett.* **2002**, *81*, 2493.
(42) Russo, M.; Campoy-Quiles, M.; Lacharmoise, P.; Ferenczi, T. A. M.; Garriga, M.; Caseri, W. R.; Stingelin, N. One-pot synthesis of polymer/inorganic hybrids: toward readily accessible, low-loss, and highly tunable refractive index materials and patterns. *J. Polym. Sci., Part B: Polym. Phys.* **2012**, *50*, 65−74.
(43) Faustini, M.; Ceratti, D. R.; Louis, B.; Boudot, M.; Albouy, P.-A.; Boissière, C.; Grosso, D. Engineering functionality gradients by dip coating process in acceleration mode. *ACS Appl. Mater. Interfaces* **2014**, *6*, 17102−17110.
(44) Lee, J.-H.; Koh, C. Y.; Singer, J. P.; Jeon, S.-J.; Maldovan, M.; Stein, O.; Thomas, E. L. 25th anniversary article: Ordered polymer structures for the engineering of photons and phonons. *Adv. Mater.* **2014**, *26*, 532−569.
(45) Park, T. J.; Hwang, S. K.; Park, S.; Cho, S. H.; Park, T. H.; Jeong, B.; Kang, H. S.; Ryu, D. Y.; Huh, J.; Thomas, E. L.; Park, C. Electrically tunable soft-solid block copolymer structural color. *ACS Nano* **2015**, *9*, 10518−10527.
(46) Chiang, Y.-W.; Chou, C.-Y.; Wu, C.-S.; Lin, E.-L.; Yoon, J.; Thomas, E. L. Large-area block copolymer photonic gel films with solvent-evaporation-induced red- and blue-shift reflective bands. *Macromolecules* **2015**, *48*, 4004−4011.
(47) Calvo, M. E.; Colodrero, S.; Hidalgo, N.; Lozano, G.; Lopez-Lopez, C.; Sanchez-Sobrado, O.; Miguez, H. Porous one dimensional photonic crystals: novel multifunctional materials for environmental and energy applications. *Energy Environ. Sci.* **2011**, *4*, 4800−4812.
(48) Calvo, M. E.; Colodrero, S.; Rojas, T. C.; Anta, J. A.; Ocaña, M.; Míguez, H. Photoconducting bragg mirrors based on TiO_2 nanoparticle multilayers. *Adv. Funct. Mater.* **2008**, *18*, 2708−2715.
(49) Puzzo, D. P.; Scotognella, F.; Zavelani-Rossi, M.; Sebastian, M.; Lough, A. J.; Manners, I.; Lanzani, G.; Tubino, R.; Ozin, G. A. Distributed feedback lasing from a composite poly(phenylene vinylene)−nanoparticle one-dimensional photonic crystal. *Nano Lett.* **2009**, *9*, 4273−4278.
(50) Lotsch, B. V.; Ozin, G. A. Photonic clays: a new family of functional 1D photonic crystals. *ACS Nano* **2008**, *2*, 2065−2074.
(51) Jiménez-Solano, A.; Galisteo-López, J. F.; Míguez, H. Fine tuning the emission properties of nanoemitters in multilayered structures by deterministic control of their local photonic environment. *Small* **2015**, *11*, 2727−2732.
(52) Mao, G.; Andrews, J.; Crescimanno, M.; Singer, K. D.; Baer, E.; Hiltner, A.; Song, H.; Shakya, B. Co-extruded mechanically tunable multilayer elastomer laser. *Opt. Mater. Express* **2011**, *1*, 108−114.
(53) Song, H.; Singer, K.; Wu, Y.; Zhou, J.; Lott, J.; Andrews, J.; Hiltner, A.; Baer, E.; Weder, C.; Bunch, R.; Lepkowicz, R.; Beadie, G. Layered Polymeric Optical Systems Using Continuous Coextrusion. *Proc. SPIE 7467, Nanophotonics and Macrophotonics for Space Environments III*; San Diego, CA, San Diego, CA, 2009; p 74670A.
(54) Fornasari, L.; Floris, F.; Patrini, M.; Canazza, G.; Guizzetti, G.; Comoretto, D.; Marabelli, F. Fluorescence excitation enhancement by Bloch surface wave in all-polymer one-dimensional photonic structure. *Appl. Phys. Lett.* **2014**, *105*, 053303.
(55) Bellingeri, M.; Chiasera, A.; Kriegel, I.; Scotognella, F. Optical properties of periodic, quasi-periodic, and disordered one-dimensional photonic structures. *Opt. Mater.* **2017**, *72*, 403−421.
(56) Monguzzi, A.; Scotognella, F.; Meinardi, F.; Tubino, R. Lasing in one dimensional dye-doped random multilayer. *Phys. Chem. Chem. Phys.* **2010**, *12*, 12947−12950.
(57) Scotognella, F.; Puzzo, D. P.; Zavelani-Rossi, M.; Clark, J.; Sebastian, M.; Ozin, G. A.; Lanzani, G. Two-photon poly(phenylenevinylene) DFB laser. *Chem. Mater.* **2011**, *23*, 805−809.
(58) Lova, P.; Manfredi, G.; Boarino, L.; Laus, M.; Urbinati, G.; Losco, T.; Marabelli, F.; Caratto, V.; Ferretti, M.; Castellano, M.; Soci, C.; Comoretto, D. Hybrid ZnO:polystyrene nanocomposite for all-polymer photonic crystals. *Phys. Status Solidi C* **2015**, *12*, 158−162.
(59) Birowosuto, M. D.; Cortecchia, D.; Drozdowski, W.; Brylew, K.; Lachmanski, W.; Bruno, A.; Soci, C. X-ray scintillation in lead halide perovskite crystals. *Sci. Rep.* **2016**, *6*, 37254.
(60) Smith, M. D.; Jaffe, A.; Dohner, E. R.; Lindenberg, A. M.; Karunadasa, H. I. Structural origins of broadband emission from layered Pb-Br hybrid perovskites. *Chem. Sci.* **2017**, *8*, 4497−4504.
(61) Hu, T.; Smith, M. D.; Dohner, E. R.; Sher, M.-J.; Wu, X.; Trinh, M. T.; Fisher, A.; Corbett, J.; Zhu, X. Y.; Karunadasa, H. I.; Lindenberg, A. M. Mechanism for broadband white-light emission from two-dimensional (110) hybrid perovskites. *J. Phys. Chem. Lett.* **2016**, *7*, 2258−2263.
(62) Lova, P.; Manfredi, G.; Boarino, L.; Comite, A.; Laus, M.; Patrini, M.; Marabelli, F.; Soci, C.; Comoretto, D. Polymer distributed bragg reflectors for vapor sensing. *ACS Photonics* **2015**, *2*, 537−543.
(63) Joannopoulos, J. D.; Villeneuve, P. R.; Fan, S. Photonic crystals: putting a new twist on light. *Nature* **1997**, *386*, 143−149.
(64) Comoretto, D. *Organic and Hybrid Photonic Crystals*; Springer: Cham, Switzerland, 2015.
(65) Smith, M. D.; Pedesseau, L.; Kepenekian, M.; Smith, I. C.; Katan, C.; Even, J.; Karunadasa, H. I. Decreasing the electronic confinement in layered perovskites through intercalation. *Chem. Sci.* **2017**, *8*, 1960−1968.
(66) Scotognella, F.; Varo, S.; Criante, L.; Gazzo, S.; Manfredi, G.; Knarr, R. J.; Comoretto, D. Spin-Coated Polymer and Hybrid Multilayers and Microcavities. In *Organic and Hybrid Photonic Crystals*; Springer: Cham, CHZ, 2015; pp 77−102.
(67) Soci, C.; Comoretto, D.; Marabelli, F.; Moses, D. Anisotropic photoluminescence properties of oriented poly(*p*-phenylenevinylene) films: Effects of the optical constants dispersion. *Phys. Rev. B: Condens. Matter Mater. Phys.* **2007**, *75*, na.
(68) Comoretto, D.; Dellepiane, G.; Cuniberti, C.; Rossi, L.; Borghesi, A.; LeMoigne, J. Photoinduced absorption of oriented poly 1,6-di(N-carbazolyl)-2,4-hexadiyne. *Phys. Rev. B: Condens. Matter Mater. Phys.* **1996**, *53*, 15653−15659.
(69) Valentina, M.; Matteo, G.; Franco, M.; Davide, C. Highly oriented poly(paraphenylene vinylene): Polarized optical spectroscopy

DOI: 10.1021/acsphotonics.7b01077
ACS Photonics 2018, 5, 867−874

under pressure. *Phys. Rev. B: Condens. Matter Mater. Phys.* **2009**, *79*, 045202.
(70) Berti, L.; Cucini, M.; Di Stasio, F.; Comoretto, D.; Galli, M.; Marabelli, F.; Manfredi, N.; Marinzi, C.; Abbotto, A. Spectroscopic investigation of artificial opals infiltrated with a heteroaromatic quadrupolar dye. *J. Phys. Chem. C* **2010**, *114*, 2403−2413.
(71) Benisty, H.; De Neve, H.; Weisbuch, C. Impact of planar microcavity effects on light extraction-Part I: basic concepts and analytical trends. *IEEE J. Quantum Electron.* **1998**, *34*, 1612−1631.
(72) Jeon, N. J.; Noh, J. H.; Kim, Y. C.; Yang, W. S.; Ryu, S.; Seok, S. I. Solvent engineering for high-performance inorganic−organic hybrid perovskite solar cells. *Nat. Mater.* **2014**, *13*, 897−903.
(73) McMeekin, D. P.; Sadoughi, G.; Rehman, W.; Eperon, G. E.; Saliba, M.; Hörantner, M. T.; Haghighirad, A.; Sakai, N.; Korte, L.; Rech, B.; Johnston, M. B.; Herz, L. M.; Snaith, H. J. A mixed-cation lead mixed-halide perovskite absorber for tandem solar cells. *Science* **2016**, *351*, 151−155.
(74) Hasan, M.; Venkatesan, S.; Lyashenko, D.; Slinker, J. D.; Zakhidov, A. Solvent toolkit for electrochemical characterization of hybrid perovskite films. *Anal. Chem.* **2017**, *89*, 9649−9653.
(75) Mark, J. E. *Polymer Data Handbook*, 2nd ed.; Oxford University Press: New York, U.S.A., 1999.
(76) Unger, K.; Resel, R.; Czibula, C.; Ganser, C.; Teichert, C.; Jakopic, G.; Canazza, G.; Gazzo, S.; Comoretto, D. Distributed Bragg Reflectors: Morphology of Cellulose Acetate and Polystyrene Multilayers. *2014 16th International Conference on Transparent Optical Networks (ICTON)*, 6−10 July 2014; pp 1−4.
(77) Frezza, L.; Patrini, M.; Liscidini, M.; Comoretto, D. *IEEE Directional Photoluminescence Enhancement in Organic Flexible Microcavities*; IEEE: New York, 2011.
(78) Born, M.; Wolf, E. *Principles of Optics*, 6th (with corrections) ed.; Pergamon Press: Oxford, 1980.
(79) *Handbook of Optical Constants of Solids*, 1st ed.; Elsevier: San Diego, 1998.

DOI: 10.1021/acsphotonics.7b01077
ACS Photonics 2018, 5, 867−874